Seasonality of sporadic physical processes driving temperature and nutrient high-frequency variability in the coastal ocean off southeast Australia

Vincent Rossi,[1] Amandine Schaeffer,[1] Julie Wood,[1] Guillaume Galibert,[2] Brad Morris,[1] Joel Sudre,[3] Moninya Roughan,[1] and Anya M. Waite[4]

[1] Physical processes forced by alongshore winds and currents are known to strongly influence the biogeochemistry of coastal waters. Combining in situ observations (moored platforms, hydrographic surveys) and satellite data (sea surface wind and sea surface height), we investigate the transient occurrence of wind-driven upwelling/downwelling and current-driven upwelling events off southeast Australia. Remote-sensed indices are developed and calibrated with multiannual time series of in situ temperature and current measurements at two shelf locations. Based on archives up to 10 years long, climatological analyses of these indices reveal various latitudinal regimes with respect to seasonality, magnitude, duration of events, and their driving mechanisms (wind or current). Generally, downwelling-favorable winds prevail in this region; however, we demonstrate that up to 10 wind-driven upwelling days per month occur during spring/summer at 28–33.5°S and up to 5 days in summer further south. Current-driven upwelling upstream of the East Australian Current separation zone (∼32°S) occurs twice as often as downstream. Using independent in situ data sets, we show that the response of the coastal ocean is consistent with our climatology of shelf processes: upwelling leads to a large range of temperatures and elevated nutrient concentrations on the shelf, maximized in the wind-driven case, while downwelling results in destratified nutrient-poor waters. The combination of these sporadic wind- and current-driven processes may drive an important part of the high-frequency variability of coastal temperature and nutrient content. Our results suggest that localized nutrient enrichment events of variable magnitude are favored at specific latitudes and seasons, potentially impacting coastal ecosystems.

1. Introduction

[2] The coastal ocean is the most biologically active part of the ocean, the most fished, and the most directly impacted by and impacting upon human activities. Despite its tremendous importance, it remains under sampled and our current understanding relies primarily on regionally focused ship-based observations and a few localized in situ time series supplemented by numerical models. Remote-sensing has given access to synoptic measurements of the global ocean, allowing the analysis of the biophysical variability of the ocean at multiple spatiotemporal scales [e.g., *Garcia-Soto et al*., 2012]. However, these measurements are limited to the surface layer and require regular validation with in situ data. In addition, most algorithms have been designed for the open ocean, and their application in coastal areas is still problematic, mainly due to the effects of shallow water depth and terrestrial inputs which complicate both the optical [*Mélin et al*., 2007] and dynamical [*Deng et al*., 2011] properties of the water column. On the other hand, in situ observations collected from ship-based surveys, moorings, and autonomous vehicles have the advantage of providing "true field data" across the whole water column. The information derived from these observational platforms, usually

Additional supporting information may be found in the online version of this article.

[1]School of Mathematics and Statistics, University of New South Wales, Sydney, New South Wales, Australia.

[2]IMOS eMarine Information Infrastructure, University of Tasmania, Hobart, Tasmania, Australia.

[3]Laboratoire d'Etudes en Géophysique et Océanographie Spatiales, CNRS/UPS/IRD/CNES, Toulouse, France.

[4]The Oceans Institute and School of Environmental Systems Engineering, University of Western Australia, Crawley, Western Australia, Australia.

Corresponding author: V. Rossi, School of Mathematics and Statistics, University of New South Wales, Sydney, NSW 2052, Australia. (vincent.rossi.ocean@gmail.com)

expensive and effort-consuming to deploy and maintain, is however space/time restricted. Thus, multisensor approaches that combine complementary in situ and remote-sensing measurements should yield an improved understanding of the coastal ocean [*Hall et al.*, 2010].

[3] Since 2008, the Australian Integrated Marine Observing System (in New South Wales) has been developed to address some of these shortcomings [*Roughan et al.*, 2010]. It is composed of an array of coastal moorings, repeated glider deployments, and high-frequency radar to examine comprehensively biophysical interactions within the East Australian Current (EAC) and the coastal waters. However, its relatively limited spatial extent and recent deployment result in a somewhat restricted spatiotemporal coverage to date [*Oke and Sakov*, 2012]. Here we use a combination of in situ and remotely sensed data sets to study the seasonal variability of physical shelf processes, and its impact on hydrography, over the southeast (SE) Australian coast.

[4] The EAC is the Western Boundary Current of the South Pacific subtropical gyre, consolidating in the Coral Sea around 15–20°S and then flowing poleward along the coast of southeastern Australia, responsible for southward transport of heat and biota [*Booth et al.*, 2007; *Roughan et al.*, 2011] (see also Figure 1). This energetic current generally flows along the narrow east Australian shelf (~20 to 80 km width south of 24°S) as an intensified jet off the shelf break from 24 to 31°S, whereupon it retroflects sharply eastward into the Tasman Sea (typically around 30–32°S, an area known as the separation zone). This dynamically unstable area is where anticyclonic (warm-core) and cyclonic (cold-core) mesoscale eddies regularly form [*Bowen et al.*, 2005] and travel southward along the coast [*Everett et al.*, 2012]. The EAC exhibits a seasonal cycle with a maximum southward transport in summer [*Ridgway and Godfrey*, 1997]. Driven by basinwide wind variability, its transport also varies at longer temporal scales [*Ridgway et al.*, 2008].

[5] This regional-scale circulation has been shown to influence coastal waters through the interaction of mesoscale eddies with the bathymetry, generally south of the separation zone [*Tranter et al.*, 1986; *McClean-Padman and Padman*, 1991; *Oke and Griffin*, 2011], and through regular EAC intrusions onto the shelf driving topographic upwelling [*Rochford*, 1975; *Oke and Middleton*, 2000]. When the EAC core encroaches onto the shelf, there is surface flooding of warm EAC waters, while the strong southward velocities enhance bottom stress in the shelf-break region, resulting in cold water intrusions [*Oke and Middleton*, 2001; *Roughan and Middleton*, 2004]. In addition, although dominant winds are downwelling-favorable in the region, wind-driven upwelling events have been observed in summer with the uplifting of cold nutrient-rich waters under poleward wind forcing [*Rochford*, 1975; *McClean-Padman and Padman*, 1991; *Griffin and Middleton*, 1992; *Middleton et al.*, 1996; *Gibbs et al.*, 1998; *Roughan and Middleton*, 2002, 2004]. More recently, an analysis of the cross-shelf dynamics highlights the important influences of alongshore current and wind on bottom temperature variability [*Schaeffer et al.*, 2013]. The two main processes leading to the uplift of cold and nutrient-rich waters onto the inner shelf are (i) wind-driven upwelling and (ii) the interactions between the southward EAC flow and the topography, referred to as current-driven upwelling. While the thermal signature of current-driven upwelling is generally confined to the subsurface, preventing the use of sea surface temperature (SST) indices [*Demarcq and Faure*, 2000], strong wind-driven events can lead to cold water reaching the surface. Both current- and wind-driven upwelling events have important biological implications with localized nutrient enrichments [*Oke and Middleton*, 2001; *Roughan and Middleton*, 2002, 2004] supporting coastal phytoplankton blooms [*Hallegraeff and Jeffrey*, 1993; *Ajani et al.*, 2000; *Thompson et al.*, 2011].

[6] The current understanding of these processes relies essentially on localized observations involving short mooring deployments and field surveys [*Suthers et al.*, 2011, and references therein]. *Bowen et al.* [2005] and *Everett et al.* [2012] investigated the dynamics of mesoscale eddies from satellite archives but did not analyze their interactions with the continental shelf. Other authors used numerical models to examine the effects of the wind on carbon fluxes [*Mac Donald et al.*, 2009] or to focus on process studies [*Oke and Middleton*, 2001; *Oke and Griffin*, 2011], but the seasonal description of sporadic upwelling events and their oceanic responses along the SE Australian shelf is still lacking. Based on multiyear in situ observations collected at several nearshore sites, *Lee et al.* [2007] and *Malcolm et al.* [2011] showed that coastal temperatures are dominated by high-frequency variability. They hypothesized it is due to sporadic upwelling events but the link between wind-driven/current-driven processes and temperature variability was not firmly established.

[7] Here we derive satellite-based indices to assess wind-driven and current-driven sporadic shelf processes. These indices are validated and calibrated using up to 3.5 years of hydrographic measurements (current and temperature) at two coastal locations. Based on a statistical "event" analysis of the satellite archives, we then present a climatological description of wind-driven upwelling/downwelling and current-driven upwelling over the SE Australian coast. Using additional in situ data sets, we suggest that the frequency of occurrence of sporadic shelf processes explains the daily/weekly variability of temperature and nutrient concentrations over a seasonal cycle.

2. Materials and Methods

2.1. Remote-Sensed Data and Upwelling Indices

2.1.1. Sea Surface Wind

[8] Remotely sensed sea surface winds (SSW) allow the study of the wind forcing and its variability. We use a composite SSW product of near-surface wind vectors on a global 0.25° grid at daily resolution. It consists of the blended observations from multiple satellites (up to six since 2002) as well as the National Centers for Environmental Prediction Reanalysis 2, which enables filling the gaps (in both time and space) of individual satellite samplings and reducing the subsampling aliases and random errors [*Zhang et al.*, 2006]. Following *Rossi et al.* [2013b], spurious near-coastal pixels have been disregarded from our analysis due to their contamination by the interpolation scheme. Further information about this data set, named BL-SSW (blended), spanning January 2000 to October 2011 (supporting information Figure S1), can be found in http://www.ncdc.noaa.gov/oa/rsad/air-sea/seawinds.html.
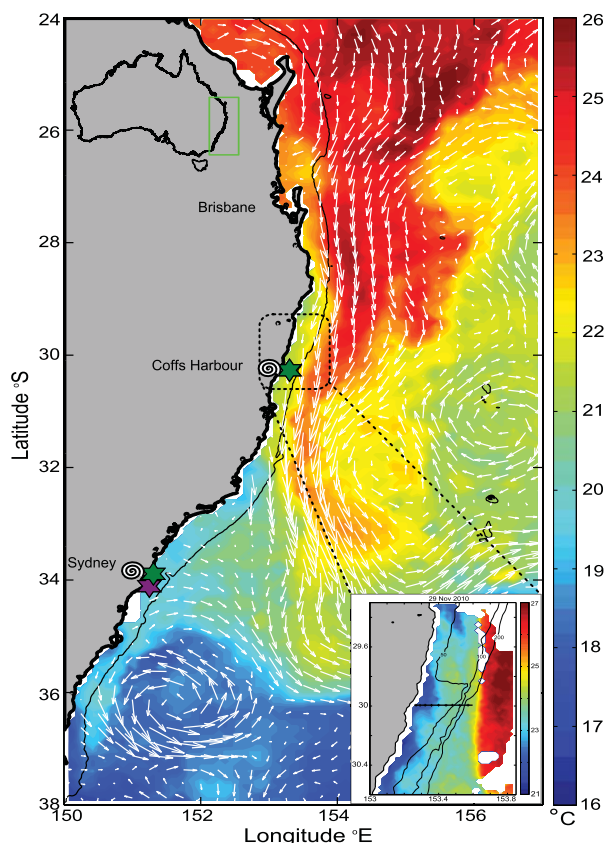
Figure 1. Sea surface temperature snapshot and corresponding surface currents (a combination of Geostrophic and Ekman currents, as described by *Sudre et al.* [2013]) on 11 October 2010. The thin black line indicates the 200 m isobath. Green stars indicate the location of the CH070 and ORS065 moorings; the purple star indicates the location of the Port Hacking National Reference Station; the "spiral" symbols show the location of the overland wind data. Top-left insert: a global map of Australia highlights the spatial extent of this study. Bottom-right insert: the black segment shows the hydrographic transect at 30°S, superimposed on a SST map of 29 November 2010.

[9] We compare BL-SSW to the wind field derived from the QuikSCAT scatterometer which measures near-surface winds at a daily frequency and 0.25° spatial resolution (level 3 products). The QS-SSW (QuikSCAT) data set was downloaded from the repository ftp://podaac-ftp.jpl.nasa.gov/OceanWinds/quikscat/ and covers only January 2000 to October 2009 (supporting information Figure S1).

2.1.2. Sea Surface Height

[10] To monitor the EAC at the shelf break, we use an improved altimetric product which consists of daily gridded sea surface height (SSH) maps produced by optimal interpolation of along-track SSH observations from all available satellite altimeters and coastal tide gauges around Australia. The long-term mean and isostatic response of the ocean to atmospheric pressure forcing are subtracted from each map, as described by *Deng et al.* [2011]. By combining altimetric data with coastal tide gauges, the relatively large errors of SSH data over shallow shelves are reduced. This data set,

named C-SSH (coastal), covers the period January 2003 to December 2011 (supporting information Figure S1) and was downloaded from the CSIRO OPeNDAP repository.

2.1.3. Wind-Driven Upwelling Index

[11] Coastal wind-driven upwelling is the process by which surface waters drift offshore through Ekman transport, compensated by a subsurface onshore flow below the Ekman layer. Many indices have been developed in the past decades to monitor upwelling activity. They are based on wind stress [*Nieblas et al.*, 2009], Ekman transport [*Bakun*, 1973; *Nykjaer and Van Camp*, 1994; *Alvarez et al.*, 2008, 2011], SST [*Demarcq and Faure*, 2000; *Alvarez et al.*, 2011], a combination of Ekman and Geostrophic cross-shore transport [*Rossi et al.*, 2013b], or more complex formulation [*Kuo et al.*, 2000]. Here we retain the Bakun Index modified after *Alvarez et al.* [2008] which is defined as the offshore Ekman transport per length of coastline, considering poleward wind as upwelling-favorable in this region. Due to the sparsity of simultaneous in situ wind measurements along the coast (e.g., buoy data and meteorological stations), we used the near-surface wind speed $W(W_x, W_y)$ from gridded SSW to compute Ekman transport over the whole SE Australian shelf as follows:

$$Q_x = \frac{\rho_A \ C_d}{\rho_w f} ||W|| \ W_y \ \text{ and } \ Q_y = -\frac{\rho_A \ C_d}{\rho_w f} ||W|| \ W_x \qquad (1)$$

with $\rho_w = 1024$ kg m^{-3} (seawater mean density), $\rho_A = 1.22$ kg m^{-3} (air density), $||W|| = \sqrt{(W_x^2 + W_y^2)}$ and the dimensionless drag coefficient C_d (taken as $C_d = 1.1 \times 10^{-3}$ for $||W|| < 6$ m s^{-1} or $C_d = 0.61 + 0.063 \ ||W||$ when $||W|| > 6$ m s^{-1}) [*Wood et al.*, 2012]. The Wind-Driven Upwelling Index (WUI) is defined as the fraction of Ekman transport strictly perpendicular to the coast [*Alvarez et al.*, 2008, 2011] by means of

$$\text{WUI} = Q_\perp = \sin(\alpha)Q_x + \cos(\alpha)Q_y \qquad (2)$$

where α is the angle of the unitary vector pointing northward to the shoreline. With this index, positive (negative) values of WUI indicate upwelling (downwelling), respectively. We study the prevalence of favorable conditions for wind-driven upwelling/downwelling by investigating the occurrence of "event," i.e., a group of consecutive days during which the WUI remains above/below the thresholds defined in section 3.1.2.

2.1.4. Current-Driven Upwelling Index

[12] In the absence of favorable wind forces, onshore near-bottom Ekman transport may occur due to high bottom stress at the shelf break induced by the southward EAC flow. This current-driven upwelling moves cold enriched water up the shelf through the bottom boundary layer (BBL) [*Oke and Middleton*, 2001; *Roughan and Middleton*, 2004]. In their numerical simulations, *Oke and Middleton* [2000] found that an increase in the along-shelf transport magnitude enhances upwelling. In addition, *Schaeffer et al.* [2013] recently revealed a linear relationship between the mean alongshore southward current and the cross-shelf bottom temperature gradient. Thus, the magnitude of the alongshore flow at the shelf break, as monitored by SSH, should be a reasonable indicator of current-

driven upwelling. The main orientation of the SE Australian shelf break is particularly variable and can be approximated as being parallel to the coastline. Hence, both zonal and meridional velocities were projected along the coastline orientation to obtain the alongshore geostrophic current v_p. Positive (negative) values of v_p indicate alongshore equatorward (poleward) velocity.

[13] Based on the thermal wind relation under geostrophic assumption, the boundary layer theory of stratified flow over a sloping shelf predicts that the onshore-shifted density field will induce a horizontal density gradient resulting in a near-bottom vertical shear. It will slow down the bottom alongshore current and in turn decreases viscous stress, thus counteracting the onshore transport [*Oke and Middleton*, 2000]. Except in specific regions where persistent bottom stress is observed (e.g., in the vicinity of prominent capes), current-driven upwelling cannot be sustained. This process led to the definition of an "upwelling shutdown time scale," of the order of a few hours to a few days in the region [*Roughan and Middleton*, 2004]. To take into account the bottom boundary layer shutdown (unsteady character), we used the acceleration of the alongshore velocity

$$a_v = \frac{\partial v_p}{\partial t} \qquad (3)$$

[14] The parameter a_v (in m d^{-2}) is computed as the finite-time difference of daily alongshore velocities and is negative when the poleward EAC is accelerating.

[15] The variability of current-driven upwelling is investigated through the occurrence of "event," defined as a group of consecutive days with forcing favorable for upwelling. To indicate so, the Current-driven Upwelling Index (CUI) requires the fulfillment of two conditions: both the poleward alongshore velocity v_p and its acceleration a_v need to be lower than the negative thresholds defined in section 3.1.2. Meeting these two criteria simultaneously is necessary to ensure that the detected current-driven upwelling events drive strong and sustained oceanic responses [*Schaeffer et al.*, 2013].

2.1.5. Climatological "Event" Analysis

[16] To study the variable occurrence of shelf processes, climatology can be built by directly averaging our satellite indices (supporting information Figure S4). These time-averaged variables are however not necessarily representative of the impacts of highly sporadic processes due to the fact that alongshore wind and to a lesser extent, alongshore current vary tremendously and regularly reverse at short time scales [*Roughan and Middleton*, 2002]. Brief episodes of upwelling-favorable winds in winter (usually dominated by downwelling conditions) and transient EAC pulses might not be detected from the time-averaged satellite indices. We therefore examine the spatiotemporal variability of sporadic shelf processes by computing a climatological occurrence of events. More specifically, (i) from the satellite indices, we extract time series of WUI, v_p, and a_v every 0.25° along the SE Australian shelf; (ii) based on the thresholds described in section 3.1.2, we detect all events, their duration, magnitude, and period of occurrence; and (iii) these characteristics are then used to build climatologies. The mean number of favorable days per month (d m^{-1}) and per year (d yr^{-1}) is computed as follows:

$$\text{Mean number of days} = \frac{\sum_{x=2}^{d_{max}} x N_x}{N_{tot}} \qquad (4)$$

where x is the number of consecutive days under upwelling-favorable conditions (i.e., the duration of an event), N_x is the total number of events lasting exactly x days, and N_{tot} is the total number of events over the period of analysis (a given month/year). The coastal ocean responds quickly (hours-day) to EAC encroachment on the shelf [*Roughan and Middleton*, 2004] and to intermittent upwelling-favorable wind events [*Wood et al.*, 2012]. However, to monitor events likely to cause a strong oceanic response and considering the daily resolution of the satellite observations, we analyze only the events lasting at least 2 days ($x \geq 2$ d). This minimum "event" duration allows the use of the steady-state Ekman equation with confidence since processes occurring at shorter time scales than the inertial period (ranging from ∼19 to ∼28 h in the region) are disregarded. The maximum event duration is prescribed as $d_{max} = 5$ days for wind-driven and current-driven processes as longer events (grouped together within the 5 day category) were rarely detected. The ratio N_5/N_{tot} gives the proportion of events lasting 5 days or more (Table 4).

2.2. In Situ Measurements and Methods

2.2.1. Overland Wind Data

[17] We used daily overland wind speed and direction provided by the Australian Bureau of Meteorology (BOM), subsampled from the hourly measurements, at Coffs Harbour (located inland, ∼18 km from the Coffs Harbour mooring) and Kurnell (located on a wharf ∼15 km from the Sydney mooring) [*Wood et al.*, 2012]. From these BOM data, the WUI was calculated as indicated in section 2.1.3 and compared with the WUI computed from SSW.

2.2.2. Moored Proxies From Two Coastal Locations

[18] In situ observations of water temperature and velocity were obtained from mooring measurements at two latitudes along the coast (Figure 1): off Sydney (ORS065, 151.3°E, 33.9°S, 65 m depth, 3 km from the coast) and off Coffs Harbour (CH070, 153.3°E, 30.3°S, 70 m depth, 15 km from the coast) [*Roughan et al.*, 2010; *Schaeffer et al.*, 2013]. Each mooring is instrumented with a bottom-mounted acoustic Doppler current profiler (ADCP) measuring horizontal current through the water column, while a string of thermistors and pressure sensors provide time series of temperature from the bottom up to 15 m from the surface. All temperature and current data are recorded every 5 min at 4 m (8 m) vertical intervals at ORS065 (CH070), respectively (Figures 2a and 3a). The tidal variability was removed by filtering the 5 min time series data as in *Schaeffer et al.* [2013], which were then subsampled at daily resolution to match the satellite products. Data are available from 1 July 2008 to 1 October 2011 (∼3.5 year time series) at ORS065 and from 1 January 2010 to 1 October 2011 (∼1.5 year time series) at CH070 (supporting information Figure S1).

[19] We defined two temperature proxies for each process of interest and analyzed their temporal anomalies. To monitor wind-driven upwelling, T-bottom was computed by averaging temperature within 30 m of the bottom (40–70 m at CH070 and 35–65 m at ORS065). To monitor current-driven upwelling, T-EAC was computed by
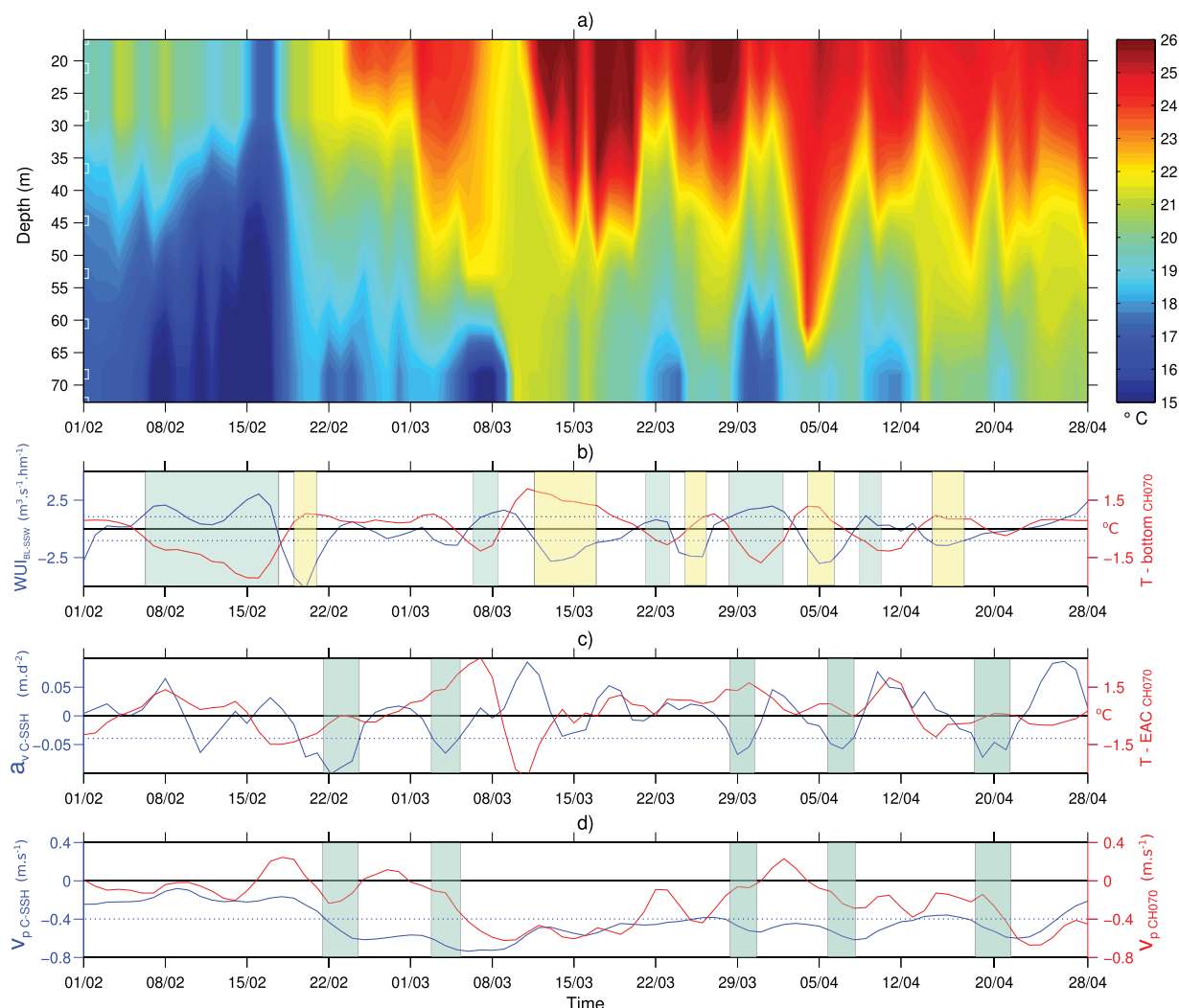
Figure 2. Vertical temperature profile, moored proxies (CH070), and remote-sensed indices from 1 February to 30 April 2010 off Coffs Harbour (30.3°S). (a) In situ temperature (white squares on the *y* axis show thermistor depths); (b) T-bottom (°C, red line, a proxy for wind-driven processes) and WUI from BL-SSW (m^3 s^{-1} hm^{-1}, blue line); (c) T-EAC (°C, red line, a proxy for current-driven upwelling) and alongshore acceleration $a_{vC\text{-}SSH}$ (m d^{-2}, blue line); and (d) alongshore velocities derived from SSH $v_{pC\text{-}SSH}$ (m s^{-1}, blue line) and measured by the mooring v_{pCH70} (m s^{-1}, red line). Green and yellow shadings indicate cold and warm water events, respectively. Blue dotted lines in Figures 2b–2d indicate the respective thresholds derived from the analysis using the entire time series. Note that for ease of visual comparison, the WUI was shifted 2 days forward (see also Table 3).

subtracting near-bottom temperature averages (55–65 m at ORS065 and 60–70 m at CH070, mimicking the BBL) from near-surface averages (15–30 m, capturing the warm EAC waters). Temporal anomalies of temperature were obtained for both proxies by applying a high-pass filter with a cutoff frequency of 15 days. According to the above definition, a cooling (warming) signal due to wind-driven upwelling (downwelling) is characterized by negative (positive) T-bottom anomalies, respectively. A current-driven upwelling is characterized by warm surface EAC waters and cooling in the BBL, resulting in positive anomalies of the proxy T-EAC. Note that these temperature proxies contain other sources of variability and thus do not reflect exclusively the occurrence of the processes of interest. We also used the alongshore ADCP velocities measured by

both moorings, v_{pORS65} and v_{pCH70} (vertically averaged and rotated appropriately) to compare with the satellite geostrophic alongshore current $v_{pC\text{-}SSH}$.

2.2.3. Hydrographic Surveys

[20] Two boat-based hydrographic surveys were carried out along a cross-shelf transect ~50 km north of Coffs Harbour (30°S, see bottom right insert in Figure 1) in late November 2010 and early June 2011. Sampling was undertaken using an automatic SBE32 carousel water sampler with 12× 5 L Niskin bottles, equipped with a SBE 911+ conductivity-temperature-depth profiler (CTD). At each station, the carousel was lowered and bottles fired at 20 to 30 m intervals from the surface to within 5 m of the seabed. For nutrient analysis, about 1 L of water from the Niskin was used to triple rinse a syringe and 0.45 μm filters, before
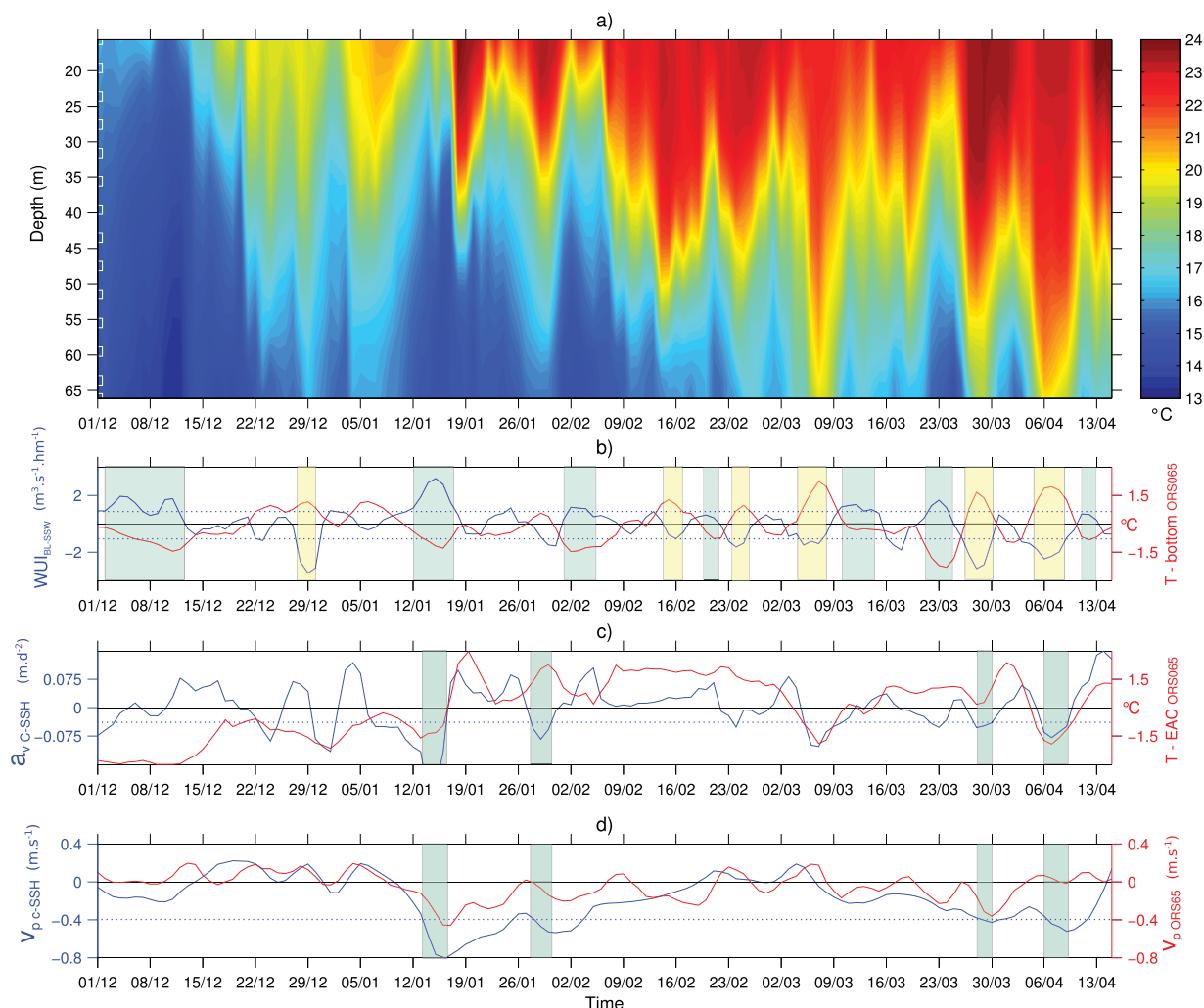
Figure 3. Same as Figure 2 with vertical temperature profile, moored proxies (ORS065), and remote-sensed indices from 1 December 2010 to 15 April 2011 off Sydney (34°S).

triple rinsing and 75% filling three 10 mL sample tubes per station depth, which were labeled and frozen. The dissolved nitrate and nitrite (hereafter "nitrate") concentrations were determined on land by colorimetric methods using an autoanalyser [*Gordon et al.*, 1995].

2.2.4. Port Hacking National Reference Station

[21] The Port Hacking National Reference Station located about 13 km off the coast of Sydney in 100 m of water (~34.1°S, 151.2°E) provides more than 50 years of standard oceanographic data collected in shelf waters. Here we used temperature and nitrate concentrations that were sampled monthly (occasionally weekly) at variable depth intervals (~10–20 m) throughout the water column and linearly interpolated every 10 m. To limit the potential of laboratory drift for the determination of nutrient concentrations, we only used post-1965 data in our analysis [*McNeil*, 2010].

3. Results

3.1. Prevalidation and Threshold Definition

3.1.1. Reliability of Remote-Sensed Data

[22] We first analyzed the reliability of the remote-sensed products over our region of interest. Note that perfect corre-

lations between the data sets are not expected since remote-sensed data are not specifically designed for the coastal ocean and in situ moored data are undoubtedly affected by local small-scale variability not resolved by satellite.

[23] From the satellite-derived offshore Ekman transport WUI, we extracted eight pixels (1° in longitude; $^{1}/_{2}$° in latitude) at close proximity to each BOM overland weather station. Comparing the WUI derived from BOM and from SSW data, all time series are well correlated at both sites ($R > 0.8$, $p < 0.05$, Table 1). The correlation between BL-SSW and BOM at Sydney is lower ($R = 0.75$), possibly related to the longer period of comparison (supporting information Figure S1). Looking at linear regression analyses (Table 2 and supporting information Figure S2), we find that both SSW products have much higher values than that of the BOM (slopes of 2.5–5.9 with small residuals), while QS-SSW has slightly higher values than BL-SSW (slope of 0.73). Note that these slopes refer to correlations of WUI so that the corresponding wind magnitude discrepancies are of the order of the squared-root correlation coefficients. Whether it is the overland site that underestimates the wind at sea, or the remotely sensed products that overestimate the wind, is out of the scope of the present

450

Table 1. Correlation Coefficients of WUI Between the Three Wind-Products Used in This Study Over the Common Period of Available Data (supporting information Figure S1) at Coffs Harbour and Sydney[a]

	BOM Versus QS-SSW	BOM Versus BL-SSW	BL-SSW Versus QS-SSW
Coffs Harbour (30.3°S)	0.86	0.82	0.86
Sydney (34°S)	0.83	0.75	0.84

[a]All correlations are significant to the 95% confidence level.

manuscript. Nevertheless, the strong correlation between remotely sensed and overland data gives us high confidence in using both SSW to assess wind variability over the east Australian coast. BL-SSW is used in the following analysis because of its extended temporal coverage (10 years of data, including the most recent years 2010 and 2011); QS-SSW was used for validation when applicable.

[24] We extracted from the geostrophic alongshore current $v_{pC\text{-}SSH}$ the pixel closest to the shelf break (200 m isobath) zonally from each mooring to compare it to the measured depth-averaged velocities v_{pORS65} and v_{pCH70}. Cross-correlation coefficients are $R = 0.37$ at CH070 (~30°S) and $R = 0.36$ at ORS065 (34°S) with a 0 day lag ($p < 0.05$; supporting information Figure S3). Despite the low coefficients due to the lack of SSH data in nearshore areas and the small-scale variability of the shelf circulation not resolved by altimetry, the significant p values and the shape of the scatterplots indicate that the strong EAC pulses lasting a few days are captured by the improved product C-SSH [*Deng et al.*, 2011].

3.1.2. Calibration of the Satellite Indices Based on Moored Data

[25] In situ temperature proxies at each site are used to derive thresholds for the remote-sensed indices. For clarity, we displayed periods of a few months in 2010 at CH070 (Figure 2) and in 2010/2011 at ORS065 (Figure 3), but the definition of thresholds and all statistics (Table 3) were calculated from the entire time series of available data (supporting information Figure S1).

3.1.2.1. Wind-Driven Upwelling

[26] Ekman theory predicts that positive WUI is associated with the upwelling of cold water onto the shelf. T-bottom is indeed inversely correlated with WUI at each site, with lagged cross-correlation spanning 0.36–0.6 with a 2 day lag ($p < 0.05$, Table 3). It suggests that the maximum temperature response to upwelling-favorable winds is observed with a lag of 2 days (or less). The correlations at both sites are slightly higher during spring/summer (Table 3), a period of strong stratification during which the detection of temperature anomalies is enhanced. Overall, periods

of clearly positive WUI (green shading) are associated with a cooling of the bottom temperature (Figures 2a, 2b, 3a, and 3b). For instance, the elevated SSW-based index (WUI > 1 m^3 s^{-1} hm^{-1}) at CH070 in 6–18 February 2010 is associated with the intrusion of cold water at the bottom (Figure 2a) and the corresponding negative temperature anomaly (T-bottom < −1°C, Figure 2b). An example of a wind-driven upwelling event at ORS065 occurs in 2–12 December 2011 with cold water at the bottom (Figure 3a) and the corresponding T-bottom anomaly (Figure 3b). To derive global thresholds, we detect all days characterized by T-bottom ≤−0.75°C in the moored time series, and we average the associated WUI values at both sites. A threshold of WUI ≥1.15 m^3 s^{-1} hm^{-1} for BL-SSW (WUI ≥ 0.85 m^3 s^{-1} hm^{-1} for QS-SSW) predicts wind-driven upwelling associated with a temperature anomaly T-bottom ≤−0.75°C. It corresponds to an upwelling-favorable wind (aligned alongshore, blowing poleward) of −8.5 m s^{-1}, i.e., an alongshore wind stress of −0.1 N m^{-2}, in good agreement with *Wood et al.* [2012].

3.1.2.2. Wind-Driven Downwelling

[27] According to Ekman theory, negative WUI indicates downwelling-favorable wind and the warming of bottom waters. Periods of strongly negative WUI (yellow shading) were generally associated with destratification of the water column and downwelling of surface warm waters (Figures 2a and 3a), leading to positive anomalies of T-bottom (Figures 2b and 3b). For instance, the negative SSW-based index (WUI < −1 m^3 s^{-1} hm^{-1}) at CH070 in 11–17 March 2010 is associated with a deepening of the warm isotherms, and thus, a positive temperature anomaly (T-bottom > 1°C; Figures 2a and 2b). A similar wind-driven downwelling event at ORS065 can be seen in 4–10 April 2011 (Figures 3a and 3b). Global thresholds are calculated by averaging the daily WUI values associated with T-bottom ≥0.75°C at both sites. A threshold of WUI ≤−1.25 m^3 s^{-1} hm^{-1} for BL-SSW (WUI ≤ −0.91 m^3 s^{-1} hm^{-1} for QS-SSW) predicts wind-driven downwelling associated with a temperature anomaly T-bottom ≥0.75°C. It corresponds to a downwelling-favorable wind (aligned alongshore, blowing equatorward) of 9 m s^{-1}, i.e., an alongshore wind stress of 0.11 N m^{-2}.

3.1.2.3. Current-Driven Upwelling

[28] While correlations between satellite indices ($v_{pC\text{-}SSH}$ and $a_{vC\text{-}SSH}$, respectively) and T-EAC were not significant (not shown), indicating not-so-trivial relationships, the CUI is satisfied when thresholds of both the alongshore current and its acceleration are met simultaneously (section 2.1.4). Looking at their temporal evolution, the periods during which they both show strongly negative values (green shading) are associated with positive T-EAC (Figures 2a, 2c, 2d, 3a, 3c, and 3d). For instance, T-EAC >1.5°C at CH070

Table 2. Linear Regressions of WUI (as in Table 1) at Coffs Harbour and Sydney[a]

	BOM Versus QS-SSW	BOM Versus BL-SSW	BL-SSW Versus QS-SSW
Coffs Harbour (30.3°S)	QS-SSW = BOM × 3.7 − 0.15 $R^2 = 0.74$	BL-SSW = BOM × 5.9 − 0.45 $R^2 = 0.67$	QS-SSW = BL-SSW × 0.73 − 0.25 $R^2 = 0.74$
Sydney (34°S)	QS-SSW = BOM × 2.5 − 0.15 $R^2 = 0.69$	BL-SSW = BOM × 3.9 − 0.5 $R^2 = 0.65$	QS-SSW = BL-SSW × 0.73 − 0.35 $R^2 = 0.71$

[a]Scatterplots are displayed in supporting information Figure S2.

Table 3. Lagged Cross-Correlation Coefficients of WUI Versus T-Bottom at Each Mooring (CH070, ORS065) Over the Common Period of Available Data (Supporting Information Figure S1) and Over the Summer Months Only[a]

	Entire Time Series		November-March	
	WUI$_{BL-SSW}$ Versus T-Bottom	WUI$_{QS-SSW}$ Versus T-Bottom	WUI$_{BL-SSW}$ Versus T-Bottom	WUI$_{QS-SSW}$ Versus T-Bottom
CH070 (30.3°S)	−0.36 (−2 d)	No data	−0.44 (−2 d)	No data
ORS065 (34°S)	−0.53 (−2 d)	−0.5 (−2 d)	−0.58 (−2 d)	−0.6 (−2 d)

[a]All correlation values are significant to the 95% confidence level.

in 1–8 March 2010 is associated with strong southward EAC velocity ($v_{pC\text{-}SSH} < -0.5$ m s^{-1}) in acceleration phase ($a_{vC\text{-}SSH} < -0.05$ m d^{-2}). The vertical temperature profile is characterized by warm surface waters and cold water intrusion at the bottom (BBL $\sim$10–15 m), representing a typical current-driven upwelling (Figures 2a, 2c, and 2d). Note that the southward current at the mooring is measured a few days later, probably due to the later intrusion of the EAC at the inner shelf. An example of a current-driven upwelling event at ORS065 occurred in 28 January to 2 February 2011 (Figures 3a, 3c, and 3d). As per the wind-driven processes, global thresholds are obtained by averaging the daily values of $v_{pC\text{-}SSH}$ and $a_{vC\text{-}SSH}$ associated with T-EAC $\geq$1°C. The thresholds $v_{pC\text{-}SSH} \leq -0.4$ m s^{-1} and $a_{vC\text{-}SSH} \leq -0.045$ m d^{-2} (i.e., -5.2×10^{-7} m s^{-2}) predict current-driven upwelling associated with a temperature anomaly T-EAC $\geq$1°C. Note that weak current-driven upwelling events are observed at times when our indices do not reach the prescribed thresholds, suggesting their occurrence might be underestimated.

3.2. Spatiotemporal Variability of Wind- and Current-Driven Processes Over the Southeast Australian Continental Shelf

[29] Based on these thresholds, we built "event" climatologies of sporadic shelf processes (section 2.1.5) using the entire satellite archives (Figures 4–6).

3.2.1. Wind-Driven Upwelling

[30] The mean number of days favorable for wind-driven upwelling varies between 0 and 10 days per month (d m^{-1}) along the whole SE Australian shelf (Figure 4a). Three latitudinal regimes are observed: from 25 to 28°S, there are upwelling-favorable conditions from August to December with 3–6 d m^{-1} during spring and less than 2 d m^{-1} the rest of the year; from 28 to 33.5°S (including Coffs Harbour), the upwelling season spans August–February, reaching its maximum of 7–10 d m^{-1} from September to December and $\leq$3 d m^{-1} otherwise; from 33.5 to 38°S (including Sydney), the maximal occurrence of wind-

Table 4. Proportion of Event Lasting 5 Days or More at Three Latitudes Along the SE Australian Coastline, as Detected Using the Full Satellite Archives

	Wind-Driven Upwelling	Wind-Driven Downwelling	Current-Driven Upwelling
26°S	6%	48%	15%
30°S	24%	37%	47%
34°S	4%	31%	24%

driven upwelling (3–5 d m^{-1}) is shifted from late November to March. These patterns are consistent in both SSW products (Figure 4a), except for a small discrepancy seen from 34.5 to 38°S. Those three latitudinal regimes are also reflected in the mean duration of events (Table 4). In the most southern and northern latitudes, only 4–6% of events last $\geq$5 days, whereas up to 24% do so over the central region, especially in spring/summer. A large majority of events ($\geq$75%) are short lasting (2–4 days).

[31] Consistently in both SSW products, there are on average 20–55 days per year (d yr^{-1}) favorable for wind-driven upwelling with similar latitudinal regimes (Figure 4b). In the northern region, there are $\sim$20 d yr^{-1} based on BL-SSW, varying from 15 d yr^{-1} at 25°S to 35 d yr^{-1} at 28°S in QS-SSW. From 28 to 33°S, it spans 35–55 d yr^{-1} (maximum at 29–31°S) in BL-SSW, while it is relatively constant (40–50 d yr^{-1}) in QS-SSW. The southern regions (33–38°S) are characterized by 20–35 d yr^{-1} favorable for wind-driven upwelling based on BL-SSW and about 30–40 d yr^{-1} in QS-SSW. Note that the number of upwelling events and their mean duration are the most important factors explaining the latitudinal gradient described above since the mean amplitude of the wind during the events was comparable at all latitudes (not shown).

3.2.2. Wind-Driven Downwelling

[32] There are on average between 3 and 15 d m^{-1} favorable for wind-driven downwelling, with the emergence of two latitudinal regimes (Figure 5a). From 25 to 29°S, downwelling conditions are observed in January–August with 8–15 d m^{-1} during summer/autumn/winter and $\leq$6 d m^{-1} in spring. From 29 to 38°S (including Sydney and Coffs Harbour), the maximum occurrence of downwelling condition spans March–September (austral autumn/winter) with 10–15 d m^{-1} in May–July and less than 8 d m^{-1} the rest of the year. Overall, patterns are consistent in both SSW products (Figure 5a). Note that the most favorable latitude/time window for upwelling (28–32°S/September–December) does not match the least favorable window for downwelling (31–36°S/November–March). In contrast with wind-driven upwelling, there are 30–50% of downwelling events lasting $\geq$5 days, with slightly higher proportions at low latitudes (Table 4).

[33] Annually, the mean number of days favorable for wind-driven downwelling varies between 60 and 110 d yr^{-1} (Figure 5b). Using BL-SSW, it is almost constant along the whole coast with $\sim$100 d yr^{-1} of downwelling, which is about twice as much as the annual mean of wind-driven upwelling days. Based on QS-SSW, the most northern and southern regions (25–29°S and 36–38°S) show the
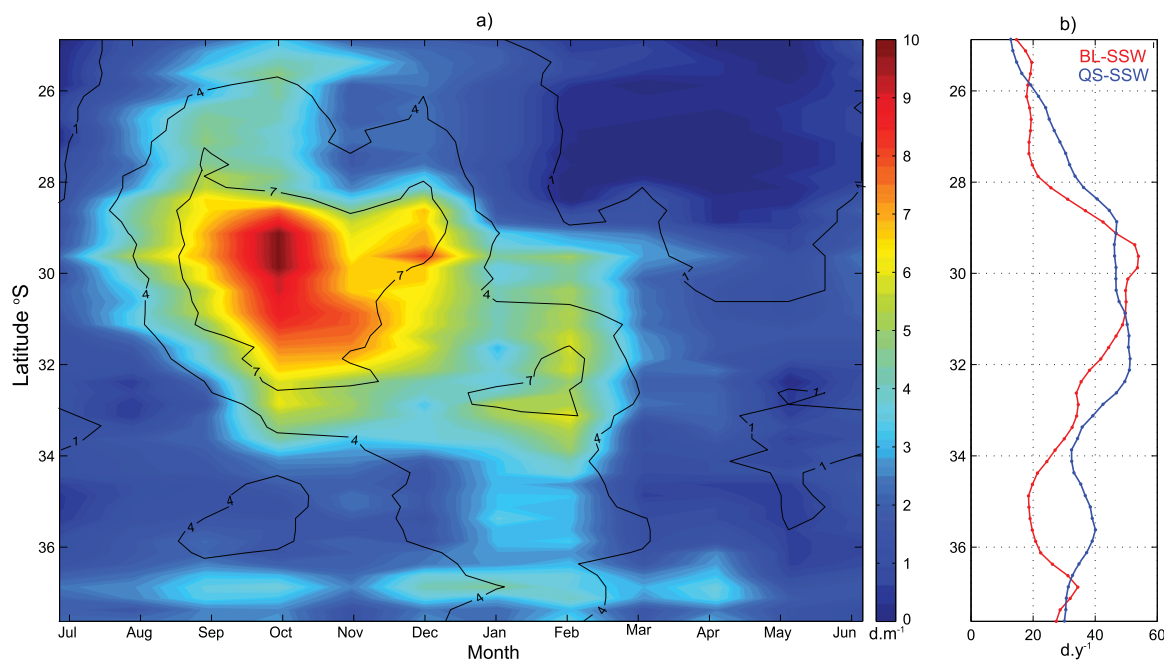
Figure 4. Spatiotemporal variability of wind-driven upwelling over the SE Australian shelf as deduced from the WUI analysis. (a) Hovmöller diagram (latitude versus time) of the mean number of wind-driven upwelling days per month (d m^{-1}) computed from BL-SSW over 2000–2008. Black contours were computed from QS-SSW. (b) Mean number of wind-driven upwelling days per year (d yr^{-1}) versus latitude (every 0.25°) as derived from BL-SSW (red) and QS-SSW (blue).

highest occurrence of downwelling winds (100 d yr^{-1}) that are less frequent (70–80 d yr^{-1}) within 29–36°S.

3.2.3. Current-Driven Upwelling

[34] There are 0–8 d m^{-1} favorable for current-driven upwelling along the whole SE Australian shelf (Figure 6a). Two latitudinal regimes are clearly delimited by the EAC separation zone at 32°S in summer/autumn and 32.5°S in winter/spring. From 25 to 32°S, there are favorable conditions for current-driven upwelling almost all year-round (1–8 d m^{-1}) with local maximum occurring in spring/ summer. From 32 to 38°S, current-driven upwelling is less favored than in the northern regions with up to 4–5 d m^{-1} observed in spring/summer (October–March) only. Depending on latitude, 10–50% of current-driven upwelling events last ≥5 days (Table 4), with longer events generally observed over narrow shelves upstream of the EAC separation point (e.g. at 30°S). It is however unclear if this dynamical process can be sustained for such long periods of time (see section 5).

[35] The annual mean number of days favorable for current-driven upwelling spans 10–60 d yr^{-1} (Figure 6b). A striking difference is observed between the northern and southern regions: 30–60 d yr^{-1} from 25 to 32.5°S but only 15–30 d yr^{-1} south of the EAC separation point (32.5– 38°S). Note also the particularly low occurrence of current-driven upwelling from 32.5 to 33.5°S, possibly related to sharp change of the shelf-break orientation limiting the occurrence of EAC intrusions there.

3.3. Oceanic Response: Temperature and Nutrient Variability

[36] Previous analyses highlight several latitude/time windows in which specific sporadic processes are favored, while their impact on the shelf hydrography is not clear yet. To address this, independent in situ data sets are used to examine the variability of temperature, density, and nutrient concentrations in light of the climatological description of shelf processes. We focus on nitrate which is considered as the limiting macronutrient in the region [*Condie and Dunn*, 2006].

3.3.1. Sydney (34°S)

[37] Historical data measured off Sydney were used to compute weekly climatological boxplots of temperature and nitrate concentrations between 30 and 60 m (Figure 7). The surface mixed layer was not included in our analysis to limit the influence of air-sea processes on temperature variability and of nutrient uptake by phytoplankton on nutrient concentrations. We also disregarded the near-bottom layer to reduce the effects of near-bottom remineralization on nitrate variability. From May to mid-July, a period dominated by downwelling winds, subsurface temperatures show small variations with [Q_5; Q_{95}], hereafter referred to as 90% of the measurements, spanning 2–3°C (Figure 7a), corresponding to a density range of 0.5 kg m^{-3} (not shown). This is associated with the lowest nitrate content with median values ranging from 1 to 2.2 μmol L^{-1} and 90% of the concentrations <4 μmol L^{-1} (Figure 7b). From mid-July to August, the amplitude of variability increases, and 90% of the measurements range over 6 μmol L^{-1} for nitrate and 4°C for temperature (1 kg m^{-3}), possibly explained by the moderate occurrence of current-driven upwelling. From September to November, highly variable but moderate median nitrate concentrations (∼2–5 μmol L^{-1}) are observed. Meanwhile, 90% of the temperature values span 4–5°C (1–1.5 kg m^{-3}) with the lower whiskers extending to 14°C. These observations are consistent with
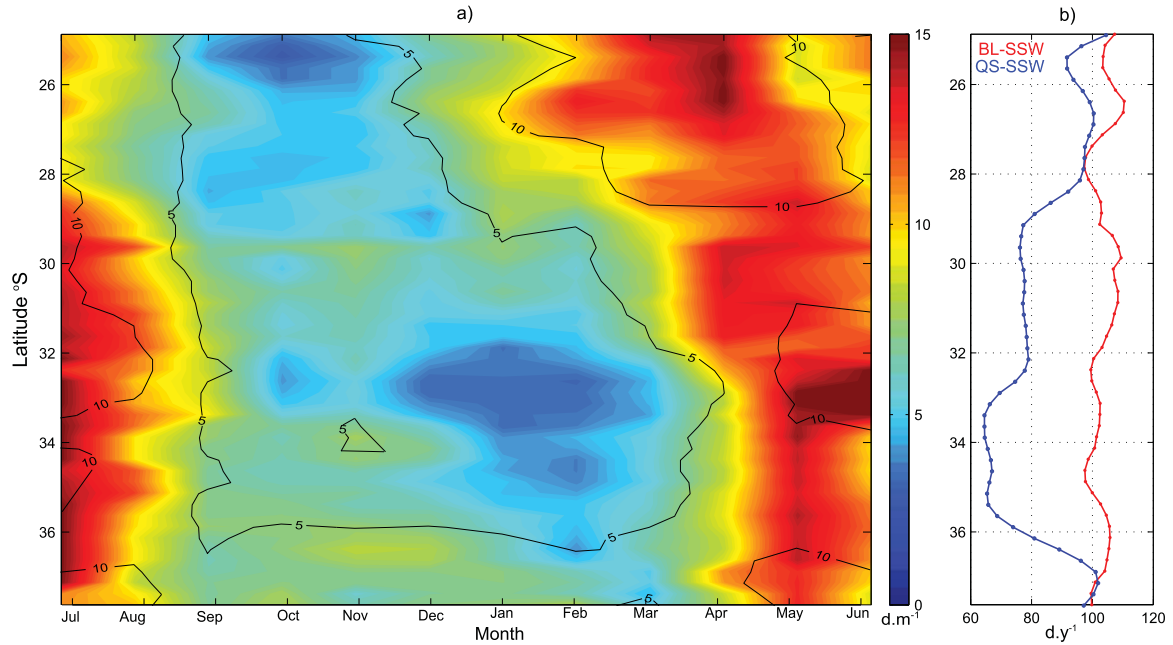
Figure 5. Spatiotemporal variability of wind-driven downwelling over the SE Australian shelf as deduced from the WUI analysis. (a) Same as Figure 4 except for the mean number of wind-driven downwelling days per month. (b) Same as Figure 4 except for the mean number of wind-driven downwelling days per year.

the onset of the wind-driven upwelling season and the moderate occurrence of current-driven upwelling. The largest variability in shelf hydrography occurs from December through to mid-April: temperature varies over 9°C (2–3 kg m^{-3}), associated with the largest variability in nitrate (0–12 µmol L^{-1}) and the highest median (∼3–7 µmol L^{-1}). Although other processes neglected in our analysis could play a role (see sections 4 and 5), this period coincides very well with the maximum occurrence of wind- and current-driven upwelling in the region. Note that outliers are present all year-round, suggesting that exceptional upwelling/downwelling events may affect temperature and nitrate concentrations even during the not-so-favorable seasons.
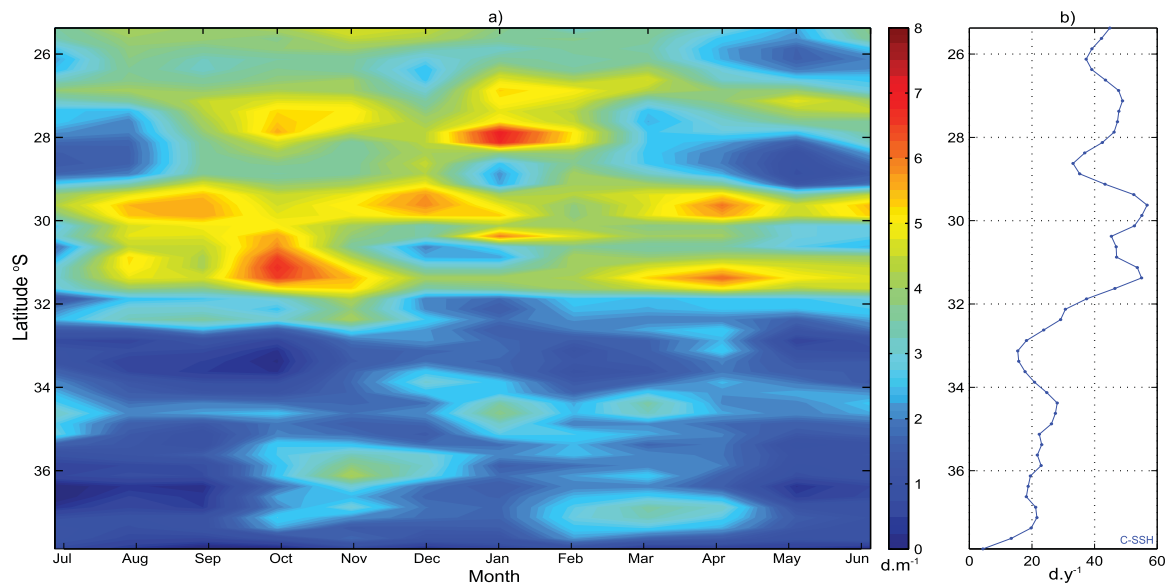

Figure 6. Spatiotemporal variability of current-driven upwelling over the SE Australian shelf as deduced from the CUI analysis based on the C-SSH archive (2003–2011). (a) Same as Figure 4 except for the mean number of favorable days for current-driven upwelling per month. (b) Mean number of favorable days for current-driven upwelling per year versus latitude (every 0.25°).
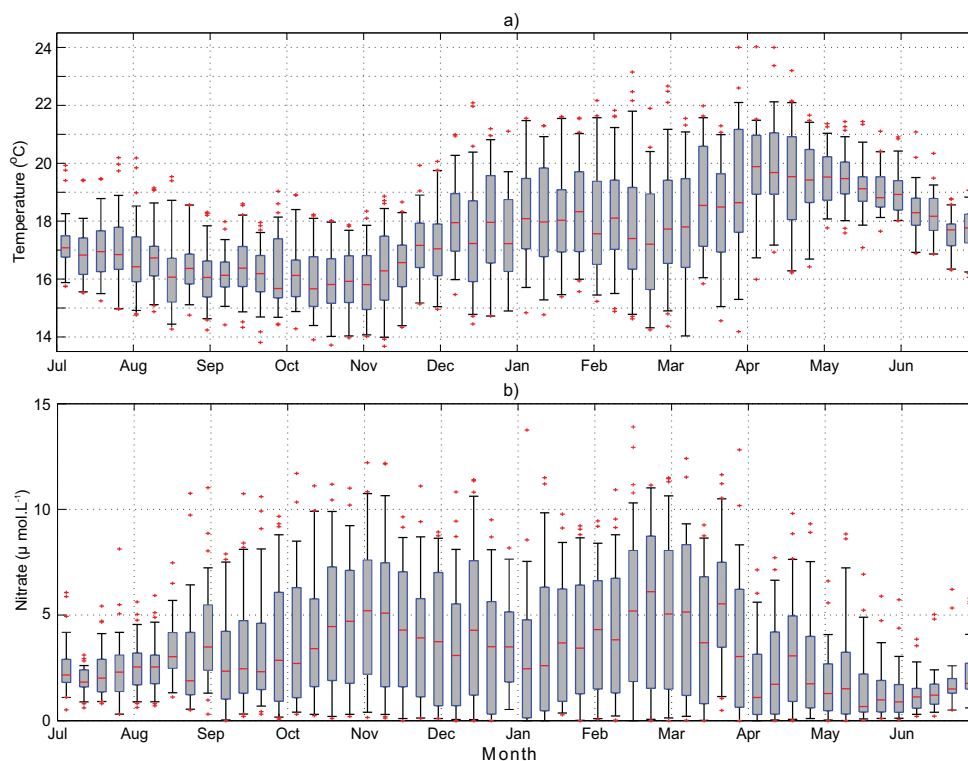
Figure 7. Weekly climatology of hydrographic data (1965–2010) collected at the 100 m Port Hacking National Reference Station. Data are from 30 to 60 m with (a) temperature in °C and (b) nitrate concentration in μmol L^{-1}. For each boxplot the central red bar is the median, the edges of the box are the 25th (Q$_{25}$) and 75th percentiles (Q$_{75}$), the whiskers extend to the 5th (Q$_5$) and 95th (Q$_{95}$) percentiles, and red crosses are "outliers."

3.3.2. Coffs Harbour (30.3°S)

[38] Temperature, density, and nitrate data collected in late 2010 and mid-2011 along a cross-shelf section located ~50 km north of Coffs Harbour (Figure 8) are in accord with the dominant physical processes suggested by the remote-sensed analysis (supporting information Figure S5).

3.3.2.1. Signature of a Wind-Driven Upwelling Event

[39] Satellite indices indicate a wind-driven upwelling in late November to early December 2010 with positive WUI (1–3 m^3 s^{-1} hm^{-1}) during about 10 days (supporting information Figure S5a). In situ data collected 3 days after the onset of favorable wind forcing reveal an intense upwelling signal (Figure 8a, see also the SST map, bottom right insert of Figure 1): cold/dense nearshore waters at the surface pushed warm/lighter waters offshore. Enriched bottom waters, bounded by the 1025.5 kg m^{-3} isopycnal, reveal an upward displacement >30 m over the 30 km long cross section. This upwelling event is characterized by high nitrate concentrations (5–10 μmol L^{-1}) brought at the surface/coast from deeper waters, while the surface offshore waters are depleted (<2 μmol L^{-1}). The ranges of temperature (7°C) and density (2.5 kg m^{-3}) observed at the inner shelf are comparable to those off Sydney during the wind-driven upwelling season (December–April, Figure 7a).

3.3.2.2. Signature of a Wind-Driven Downwelling Event

[40] The temporal evolution of satellite indices suggests the occurrence of a wind-driven downwelling in late May/early June 2011 with a strongly negative WUI (−8 to −4 m^3 s^{-1} hm^{-1}) for about 10 days (supporting information Figure S5b). Data collected on 29 May shows a clear downwelling signal (Figure 8b) with a downward slope of the isopycnals toward the coast (~15 m vertical displacement for the isopycnal 1024.75 kg m^{-3}) associated with a northward coastal flow at the inner shelf (supporting information Figure S5c1). The stratification is reduced over the shelf as shown by the small ranges of density (~1 kg m^{-3}) and temperature (~1.5°C). Similar to the winter conditions off Sydney (Figure 7a), this resulted in low nitrate levels on the shelf in the top 70 m (<2 μmol L^{-1}). Note that submesoscale processes superimposed their signatures on the shelf-scale downwelling signal (see section 5), resulting in finer-scale (~km) variability in these fields [*Rossi et al.*, 2013a].

3.3.2.3. Signature of a Current-Driven Upwelling Event

[41] The latter downwelling event was preceded (19–26 May) and immediately followed (5–10 June) by weak wind forcing and the EAC intrusion on the shelf, as suggested by the poleward velocities v_{pCH70} and $v_{pC\text{-}SSH}$ (supporting information Figure S5c1). The evolution of $a_{vC\text{-}SSH}$ and T-EAC (supporting information Figure S5c2) confirms that conditions favoring current-driven upwelling were met twice, on 25 May and to a lesser extent on 6 June. Although there was no apparent perturbation of the surface stratification, a slight upward slope of the near-bottom isopycnals (15 m uplift of 1025 kg m^{-3}) was observed on 6 June (Figure 8c). These dense/cold bottom waters brought high
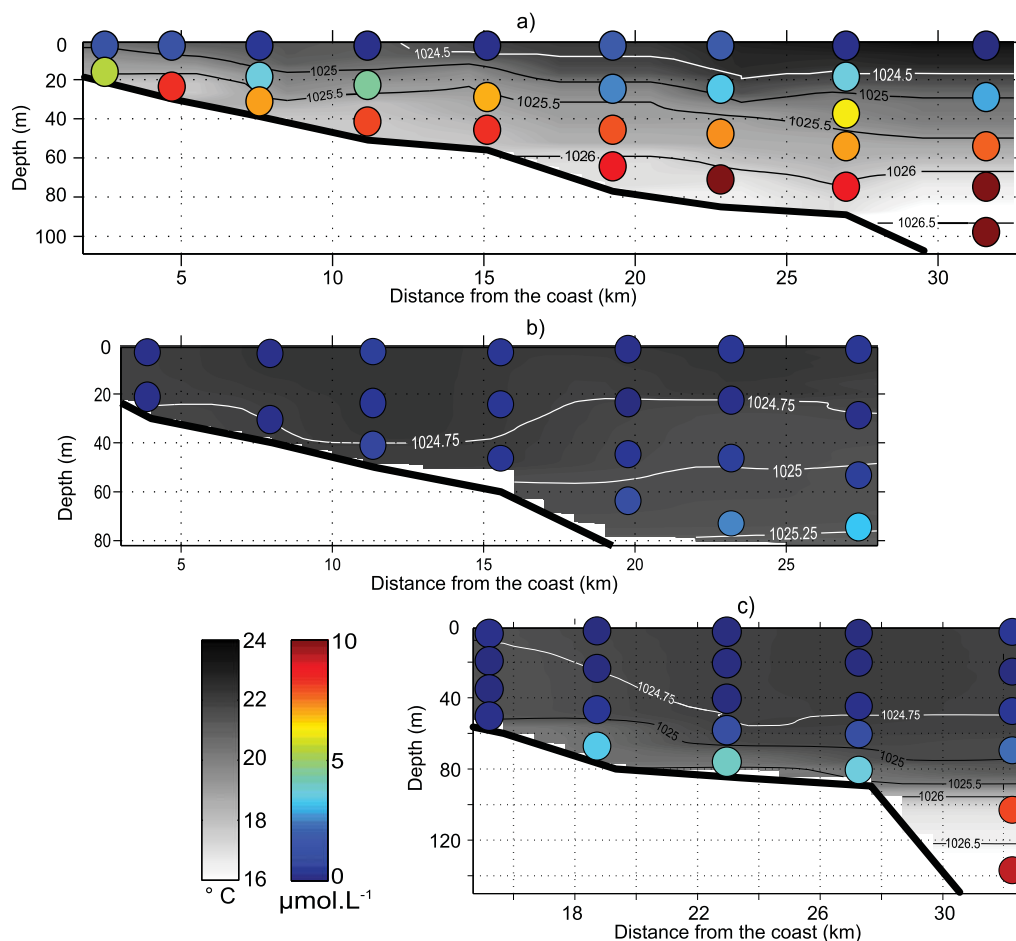
Figure 8. Hydrographic data collected at 30°S (Coffs Harbour) during (a) wind-driven upwelling, (b) wind-driven downwelling, and (c) current-driven upwelling events. The temporal evolution of the corresponding satellite indices (WUI$_{BL\text{-}SSW}$, $v_{pC\text{-}SSH}$, $a_{vC\text{-}SSH}$) and moored proxies (T-bottom, T-EAC, v_{pCH70}) is provided in supporting information Figure S5. (a) Cross-shelf section of temperature (°C, colored) and density (kg m^3, contoured) as measured by CTD on 29 November 2010 along nine stations. The colored circles represent the nitrate concentrations (μmol L^{-1}) obtained from water sampling. (b) Cross-shelf section of hydrographic data collected on 29 May 2011 along seven stations, as in Figure 8a. (c) Cross-shelf section of hydrographic data sampled on 6 June 2011 along five stations, as in Figure 8a.

nutrient concentrations (3–5 μmol L^{-1}) onto the shelf toward the coast (Figure 8c), while the top 40 m remains <1 μmol L^{-1}. Note that the vertical displacement of isopycnals (15 m) as well as the inner-shelf ranges of temperature (4°C), density (1.25 kg m^{-3}), and nitrate concentrations (1–5 μmol L^{-1}) are about half of what was observed during the November 2009 wind-driven upwelling event.

[42] It is worth mentioning that since our sampling did not take place during the period of maximal forcing (as derived from the satellite indices), we might be potentially underestimating the hydrological impact of each of the three processes of interest.

4. Uncertainties and Caveats

4.1. Postvalidation and Nonresolved Processes

[43] We used in situ moored data of two sites to calibrate satellite indices (global thresholds definition) which then

allowed us to study the occurrence of shelf processes over the entire SE Australian coastline. Conversely, *Oke and Sakov* [2012] used synoptic satellite data to investigate the spatial area effectively monitored by a localized in situ observation array. To estimate a posteriori the uncertainty of our approach, we now identified from the satellite indices each event matching our criteria, and we computed from the in situ proxies the proportion of days effectively characterized by the expected temperature anomalies.

[44] Based on the threshold WUI$_{BL\text{-}SSW}$ ≥1.15 m^3 s^{-1} hm^{-1} during periods ≥2 days, 34% (36%) of the selected days for wind-driven upwelling are effectively characterized by T-bottom ≤−0.75°C, while 70% (82%) reveal negative temperature anomalies T-bottom <0°C at CH070 (ORS065, respectively). Using the threshold WUI$_{BL\text{-}SSW}$ ≤−1.25 m^3 s^{-1} hm^{-1} for periods ≥2 days, 21% (32%) of the wind-driven downwelling days are effectively characterized by T-bottom ≥0.75°C and 60% (75%) reveal positive temperature anomalies at CH070 (ORS065,

respectively). Using both thresholds $v_{pC\text{-}SSH} \leq -0.4$ m s^{-1} and $a_{vC\text{-}SSH} \leq -0.045$ m d^{-2} for periods ≥ 2 days, 20% (18%) of the current-driven upwelling days are effectively characterized by T-EAC $\geq 1°$C, while 61% (52%) reveal positive temperature anomalies, at CH070 (ORS065, respectively).

[45] Overall, 60–80% of the days detected by our remote-sensed approach for wind-driven processes reveal a temperature change in the predicted direction (cooling for upwelling and warming for downwelling). Further improvements of the WUI could be achieved by using a wind product with higher spatiotemporal resolution to take into account (i) the subdaily variations of the wind field, especially the persistent summer sea breeze [*Gibbs*, 2000]; and (ii) the small-scale variations of the wind due to near-shore orographic effects. Note that land-based BOM weather stations are not appropriate to assess the nearshore winds because of their varying characteristics (such as their distance to the ocean and local sheltering effects) [*Wood et al.*, 2012]. The lower detection success associated with the CUI indicates higher uncertainties in the proxy T-EAC and the CUI formulation. To improve the CUI and derive a more relevant temperature proxy for current-driven upwelling, modeling studies could help identify the surface expression of this process and describe its thermal response more precisely.

[46] Importantly, the thresholding procedure leads to different results when both sites are considered separately. Using CH070 alone (ORS065 alone, respectively), the WUI$_{BL\text{-}SSW}$ threshold would be 1.35 m^3 s^{-1} hm^{-1} (0.65 m^3 s^{-1} hm^{-1}) for upwelling and -0.85 m^3 s^{-1} hm^{-1} (-2.1 m^3 s^{-1} hm^{-1}) for downwelling; the CUI thresholds would be $v_{pC\text{-}SSH} = -0.45$ m s^{-1} (-0.35 m s^{-1}) and $a_{vC\text{-}SSH} = -0.04$ m d^{-2} (-0.05 m d^{-2}). This suggests that a similar forcing (remotely sensed) could drive different in situ oceanic responses at each location. Another possibility is that the thresholding procedure was not applied to the same temporal period (supporting information Figure S1). Different thresholds are most likely explained by local factors which introduce additional variability, which may be responsible for the different linear regressions found between in situ and satellite data at both coastal sites (Table 2). Such small-scale factors were also invoked by *Malcolm et al.* [2011] to explain the contrast in high-frequency variability of coastal temperature measured at several sites situated within a 50 km radius. They include the cross-shelf location of the observation, the local topography, and the numerous submesoscale processes such as eddies, filaments and fronts [*Rossi et al.*, 2013a].

4.2. Interactions Between Shelf Processes

[47] Our analysis has considered each of the different mechanisms (wind- and current-driven) in isolation; however, in reality a number of different processes can influence the water column simultaneously. Hence, there are potentially positive/negative interactions between them, reinforcing/erasing the expected oceanic response. For instance, it is known that the poleward flowing EAC "preconditions" shelf waters by uplifting the isotherms, which can then be more easily raised to the surface under the influence of upwelling-favorable wind forcing [*Gibbs et al.*, 1998; *Roughan and Middleton*, 2002; *Schaeffer*

et al., 2013]. This is observed at ORS065 in early February 2011: despite a moderate WUI, this wind-driven upwelling event resulted in a strong temperature response probably enhanced by the occurrence of a current-driven upwelling in late January (Figure 3). On the other hand, one such negative interaction is a current-driven upwelling counteracted by the simultaneous occurrence of downwelling-favorable winds. It is seen, for example, at ORS065 from 5 to 11 April 2011: our SSH-based indices favor a current-driven event (Figures 3c and 3d), potentially cooling bottom waters, while the SSW-based index indicates a strong downwelling event (Figure 3b), consequently erasing the thermal signature of the former process.

[48] In addition, both temperature and velocity in situ time series are significantly autocorrelated over a few days (not shown). This will affect in turn both the timing and amplitude of the temperature response of a given event. For instance, the satellite indices suggested the occurrence of current-driven upwelling at CH070 in 19–22 April 2010 (Figure 2). Although a weak cooling of the near-bottom waters is noticeable on 20–22 April, T-EAC increased only slightly due to the prevalence of downwelling-favorable forcing immediately prior (15–19 April).

[49] The dominant EAC flow dictates that temperature and velocity are also correlated in the alongshore direction as water masses are advected southward. The occurrence of favorable forcing for current-driven upwelling at a particular time/location along the coast might lead to temperature anomalies and nutrient enrichment further downstream some days later, as suggested by *Oke and Middleton* [2001]. While our analyses indicate moderate to low occurrence of upwelling off Port Stephens ($\sim 32.7°$S), the recurrent upwelling manifestations at this location [*Hallegraeff and Jeffrey*, 1993; *Ajani et al.*, 2000] could be explained by the numerous wind- and current-driven upwelling events occurring upstream (32.5–33.5°S) and the local offshoot of the EAC providing a sheltered area where advected upwelled waters may persist.

[50] Alongshore winds may also modulate the sustainability of current-driven upwelling through the shutdown time scale, i.e., the time needed for bottom Ekman force to be balanced by buoyancy gradients [*Roughan and Middleton*, 2004]. This parameter is inversely proportional to the water column stratification which, in addition to seasonal variability, is also affected by the sporadic occurrence of wind-driven downwelling (destratifying) and upwelling (stratifying) events.

5. General Discussion

5.1. Shelf Physical Processes in a Western Boundary Current

[51] Although large-scale winds are not usually upwelling-favorable in this region, we found on average 3–10 d m^{-1} of sporadic wind-driven upwelling during the austral spring/summer months. In comparison with the Iberian Peninsula semipermanent upwelling system, *Alvarez et al.* [2011] found that wind-driven upwelling events occur on average 20–30 d m^{-1} in summer/autumn and 10–15 d m^{-1} in the least favorable winter periods.

[52] Although event duration rarely exceeds 10 days, we have shown that sporadic wind-driven upwelling events do

occur in this Western Boundary Current system (15–55 d yr^{-1}) and are longer and more frequent in spring/summer. Three latitudinal regimes with distinct seasonal variability exist with favorable conditions from August to December within 25–28°S which contrast with the upwelling season from August to February within 28–33.5°S, as seen by *Rochford* [1975]. Further south (33.5–38°S), the wind-driven upwelling season is shifted from December to late March, in line with previous studies documenting wind-driven upwelling in summer [*McClean-Padman and Padman*, 1991; *Middleton et al.*, 1996; *Gibbs et al.*, 1998; *Gibbs*, 2000; *Roughan and Middleton*, 2004].

[53] As expected, downwelling conditions dominate the annual cycle along the SE Australian coast (60–120 d yr^{-1}) with distinct seasonality: they are prevalent from December to August within 25–29°S and from April to September between 29 and 38°S. Downwelling event minima do not equal upwelling event maxima, suggesting that wind reversal is a common feature of the region and thus making the "event" analysis more relevant than time-averaged indices. Although wind-driven upwelling is prominent at 29–32°S from September to January, downwelling conditions may occur intermittently during the same period, thus shortening the duration of nutrient enrichment events. In contrast within 32–35°S, wind-driven upwelling is moderately favored from December to March while downwelling events are rare, likely optimizing the impact of the shelf intrusion of enriched waters.

[54] We showed a large spatiotemporal variability (15–60 d yr^{-1}) in the mean occurrence of current-driven upwelling along the SE Australian coast with striking latitudinal difference. North of the separation point (25–32.5°S), current-driven upwelling events are favored almost all year-round with a slight local maximum in spring/summer. *Oke and Middleton* [2000] also found a greater occurrence of thermal fronts during the spring and summer periods due to an increased magnitude of southward flow at 29–32°S. South of the separation point (32.5–38°S), current-driven upwelling are less prevalent due to the not-so-frequent southward penetration of the EAC as it retroflects into the Tasman Sea at 32.5°S [*Ridgway and Godfrey*, 1997]. In the southern regions, current-driven upwelling is favored during spring and summer (October–April), in good agreement with *Tranter et al.* [1986]. The development of current-driven upwelling along this coast might also be caused by the transient pulses of southward current associated with the numerous warm-core (anticyclonic) mesoscale eddies traveling close to the shelf break between 32 and 38°S [*Everett et al.*, 2012].

5.2. Shelf-Scale Analysis of Temperature and Nutrient Variability Impacting Coastal Ecosystems

[55] The spatiotemporal variability of these shelf processes is reflected in coastal water hydrography. Wind-driven upwelling events result in a large range of coastal temperatures (6–9°C) and high nitrate concentrations (5–10 μmol L^{-1}), in good agreement with the observations of *Rochford* [1975] during upwelling off Laurieton. In comparison, moderate temperature range (4–5°C) and nitrate concentration (2–5 μmol L^{-1}) are associated with current-driven upwelling. When downwelling conditions prevail, shelf waters are quickly destratified, resulting in a very nar-

row temperature range (1–2°C) and low nitrate concentrations (<2 μmol L^{-1}). Although other factors could affect stratification and nitrate loads in shelf waters, our results suggest that wind- and current-driven processes drive an important part of their high-frequency variability.

[56] Wind variability (and the resulting temperature anomaly) is mainly driven by synoptic weather patterns in this region, with typical period from days to 1–2 weeks. This is in line with *Lee et al.* [2007] who found energy peaks in temperature records at 34–32.5°S associated with period of 7–10 days. Based on a 7 year in situ data set, *Malcolm et al.* [2011] also observed the maximum temperature variability of shelf waters at hourly/daily time scales during spring/summer at 29–31°S, in good agreement with the repeated occurrence of wind-driven upwelling from September to February. The factors influencing the occurrence of current-driven upwelling (EAC pulses and meandering, mesoscale eddy encroachment, current reversals) also vary at short time scales. Thus, nutrient enrichment driven by these processes should be limited in time (<10 days) and of variable magnitude, impacting phytoplankton composition in the region [*Armbrecht et al.*, 2013].

[57] The combination of conditions favorable for both wind- and current-driven upwelling in spring/summer at 29–32°S should result in the most intense and frequent nutrient enrichment events over the SE Australian shelf. This may explain why *Thompson et al.* [2011] reported at 29–32°S one of the highest concentrations (up to 0.15 μg L^{-1}) of *fucoxanthin* (biomarker of diatoms) along the SE Australian coast. They also pointed out that microphytoplankton (>20 μm) represent a large proportion of the communities there, while picoplankton (<2 μm) are almost absent in the region, further supporting the mesotrophic character of this coastal location. Conversely, *Thompson et al.* [2011] documented a local minimum of chlorophyll *a* north of 28°S, possibly due to the rare wind-driven upwelling but frequent downwelling events in this area. Off Sydney, low temperature ranges and moderate nitrate concentrations observed in August–November (Figure 7) could be explained by the regular wind-driven downwelling associated with occasional current-driven/wind-driven upwelling. The resulting low-but-varying nutrient concentrations favor the prevalence of middle (nano) and small-size (pico) phytoplankton there, as suggested by *Thompson et al.* [2011]. Later in the year (November–March), current- and wind-driven upwelling events are prominent, potentially driving frequent nutrient enrichments which support the recurrent phytoplankton blooms reported by *Ajani et al.* [2000] during this period.

6. Conclusions

[58] We have used two satellite data sets in association with in situ measurements to improve our understanding of biophysical interactions along the SE Australian coast. Indices derived from SSW and SSH data are used to analyze transient physical shelf processes, namely, wind-driven upwelling/downwelling and current-driven upwelling. Thresholds of remote-sensed indices were defined, and postvalidated, using multiannual time series of temperature and velocity from in situ moorings at two key coastal locations. "Event" climatologies of the occurrence of these

processes illuminated several latitudinal regimes with distinct seasonality. Using additional and independent in situ hydrographic data sets, we suggested that sporadic wind-driven/current-driven processes drive an important part of the high-frequency variability of temperature and nutrient load of coastal waters in this area. Although transient nutrient enrichments of variable amplitude can occur at any time of the year, we have demonstrated that they are particularly favored at specific latitudes/seasons, probably impacting phytoplankton biogeography and coastal ecosystems. As both the wind regimes and the EAC dynamics also vary at interannual time scales, a natural extension of this work would be to investigate the long-term variability of these processes using extended satellite data sets. Assessing the full range of variability in the coastal ocean is necessary to better comprehend its biogeochemical role and the food webs it shelters.

References

Ajani, P., R. S. Lee, T. Pritchard, and M. Krogh (2000), Phytoplankton dynamics at a long-term coastal station off Sydney, Australia, *J. Coastal Res.*, *34*, 60–73.

Alvarez, I., M. Gomez-Gesteira, M. de Castro, and J. M. Dias (2008), Spatio-temporal evolution of upwelling regime along the western coast of the Iberian Peninsula, *J. Geophys. Res.*, *113*, C07020, doi:10.1029/2008JC004744.

Alvarez, I., M. Gomez-Gesteira, M. de Castro, M. N. Lorenzo, A. J. C. Crespo, and J. M. Dias (2011), Comparative analysis of upwelling influence between the western and northern coast of the Iberian Peninsula, *Cont. Shelf Res.*, *31*, 388–399.

Armbrecht, L. H., M. Roughan, V. Rossi, A. Schaeffer, P. L. Davies, A. M. Waite, and L. K. Armand (2013), Phytoplankton composition under contrasting oceanographic conditions: Upwelling and downwelling (eastern Australia), *Cont. Shelf Res.*, doi:10.1016/j.csr.2013.11.024, in press.

Bakun, A. (1973), Coastal upwelling indices, west coast of North America, 1946–71, *Tech. Rep. NMF 671*, 103 pp., NOAA, Washington, D. C.

Booth, D. J., W. F. Figueira, M. A. Gregson, L. Brown, and G. Beretta (2007), Occurrence of tropical fishes in temperate south eastern Australia: Role of the East Australian Current, *Estuarine Coastal Shelf Sci.*, *72*, 102–114.

Bowen, M. M., J. L. Wilkin, and W. J. Emery (2005), Variability and forcing of the East Australian Current, *J. Geophys. Res.*, *110*, C03019, doi:10.1029/2004JC002533.

Condie, S. A., and J. R. Dunn (2006), Seasonal characteristics of the surface mixed layer in the Australasian region: Implications for primary production regimes and biogeography, *Mar. Freshwater Res.*, *57*(6), 569–590.

Everett, J. D., M. E. Baird, P. R. Oke, and I. M. Suthers (2012), An avenue of eddies: Quantifying the biophysical properties of mesoscale eddies in the Tasman Sea, *Geophys. Res. Lett.*, *39*, L16608, doi:10.1029/2012GL053091.

Demarcq, H., and V. Faure (2000), Coastal upwelling and associated retention indices derived from satellite SST. Application to Octopus vulgaris recruitment, *Oceanol. Acta*, *23*, 391–408.

Deng, X., D. A. Griffin, K. Ridgway, J. A. Featherstone, N. J. White, and M. Cahill (2011), Satellite altimetry for geodetic, oceanographic and climate studies in the Australian region, in *Coastal Altimetry*, edited by S. Vignudelli et al., pp. 473–508, Springer, Berlin.

Garcia-Soto, C., J. Vazquez-Cuervo, P. Clemente-Colón, and F. Hernandez (2012) Satellite oceanography and climate change, *Deep Sea Res., Part II*, 77–80, 1–9.

Gibbs, M. T. (2000), Detecting a response to weak sea breezes in the New South Wales coastal ocean, *N. Z. J. Mar. Freshwater Res.*, *34*, 669–680.

Gibbs, M. T., J. H. Middleton, and P. Marchesiello (1998), Baroclinic response of Sydney shelf waters to local wind and deep ocean forcing, *J. Phys. Oceanogr.*, *28*, 178–190.

Gordon, L. I., J. C. Jennings, A. R. Ross, and J. M. Krest (1995), A suggested protocol for continuous flow automated analysis of seawater nutrients (phosphate, nitrate, nitrite, and silicic acid) in the WOCE hydrographic program and the Joint Global Ocean Fluxes Study, in *WOCE Operations Manual*, *Tech. Rep. 93–10*, Oceanogr. Group, Woods Hole, Mass.

Griffin, D. A., and J. H. Middleton (1992), Upwelling and internal tides over the inner New South Wales continental shelf, *J. Geophys. Res.*, *97*, 14,389–14,405.

Hall, J., D. E. Harrison, and D. Stammer (Eds.) (2010), *Proceedings of OceanObs'09: Sustained Ocean Observations and Information for Society*, Venice, Italy, 21–25 September 2009, *ESA Publ.* WPP-306, doi:10.5270/OceanObs09.

Hallegraeff, G. M., and S. W. Jeffrey (1993), Annually recurrent diatom blooms in spring along the New South Wales Coast of Australia, *Aust. J. Mar. Freshwater Res.*, *44*, 325–334.

Kuo, N.-J., Q. Zheng, and C.-R. Ho (2000), Satellite observation of upwelling along the western coast of the South China Sea, *Remote Sens. Environ.*, *74*, 463–470.

Lee, R. S., S. L.Wallace, C. Holden, and K. P. Black (2007), Scaling coastal upwelling features of the East Australian Current, *J. Coastal Res.*, *50*, 1152–1162.

Mac Donald, H. S., M.E Baird, and J. H. Middleton (2009), Effect of wind on continental shelf carbon fluxes off south east Australia: A numerical model, *J. Geophys. Res.*, *114*, C05016, doi:10.1029/2008JC004946.

Malcolm, H. A., P. L. Davies, A. Jordan, and S. D. A. Smith (2011), Variation in sea temperature and the East Australian Current in the Solitary Islands region between 2001–2008, *Deep Sea Res., Part II*, *58*(5), 616–627.

McClean-Padman, J., and L. Padman (1991), Summer upwelling on the Sydney inner continental shelf: The relative roles of local wind forcing and mesoscale eddy encroachment, *Cont. Shelf Res.*, *11*, 321–345. doi:10.1016/0278-4343(91)90025-2.

McNeil, B. I. (2010), Diagnosing coastal ocean CO_2 interannual variability from a 40 year hydrographic time series station off the east coast of Australia, *Global Biogeochem. Cycles*, *24*, GB4034, doi:10.1029/2010GB003870.

Mélin, F., G. Zibordi and J-F. Berthon (2007), Assessment of satellite ocean color products at a coastal site, *Remote Sens. Environ.*, *110*(2), 192–215.

Middleton, J. H., D. Cox, and P. Tate (1996), The oceanography of the Sydney region, *Mar. Pollut. Bull.*, *33*, 124–131.

Nieblas, A-E, B. M. Sloyan, A. J. Hobday, R. Coleman, and A. J. Richardson (2009), Variability of biological production in low wind-forced regional upwelling systems: A case study off southeastern Australia, *Limnol. Oceanogr.*, *54*(5), 1548–1558.

Nykjaer, L., and L. Van Camp (1994), Seasonal and interannual variability of coastal upwelling along northwest Africa and Portugal from 1981 to 1991, *J. Geophys. Res.*, *99*, 14,197–14,208.

Oke, P. R., and D. A. Griffin (2011), The cold-core eddy and strong upwelling off the coast of New South Wales in early 2007, *Deep Sea Res.*, *58*(5), 574–591.

Oke, P. R., and J. H. Middleton (2000), Topographically induced upwelling off Eastern Australia, *J. Phys. Oceanogr.*, *30*(3), 512–531.

Oke, P. R., and J. H. Middleton (2001), Nutrient enrichment off Port Stephens: The role of the East Australian Current, *Cont. Shelf Res.*, *21*, 587–606.

Oke, P. R., and P. Sakov (2012), Assessing the footprint of a regional ocean observing system, *J. Mar. Syst.*, *105–108*, 30–51, doi:10.1016/j.jmarsys.2012.05.009.

Ridgway, K. R., and J. S. Godfrey (1997), Seasonal cycle of the East Australian Current, *J. Geophys. Res.*, *102*(C10), 22,921–22,936.

Ridgway, K. R., R. C. Coleman, R. J. Bailey, and P. Sutton (2008), Decadal variability of East Australian Current transport inferred from repeated high-density XBT transects, a CTD survey and satellite altimetry, *J. Geophys. Res.*, *113*, C08039, doi:10.1029/2007JC004664.

Rochford, D. J. (1975), Nutrient enrichment of East Australian coastal waters: 2. Laurieton upwelling, *Aust. J. Mar. Freshwater Res.*, *26*, 233–243.

Rossi, V., V. Garçon, J. Tassel, J. B. Romagnan, L. Stemmann, F. Jourdin, P. Morin, and Y. Morel (2013a), Cross-shelf gradient in the Iberian Peninsula Upwelling System: Impact of a mesoscale filament, *Cont. Shelf Res.*, *59*, 97–114.

Rossi, V., M. Feng, C. Pattiaratchi, M. Roughan, and A. M. Waite (2013b), On the factors influencing the development of sporadic upwelling in the Leeuwin Current System, *J. Geophys. Res.*, *118*, 1–14, doi:10.1002/jgrc.20242.

Roughan, M., and J. H. Middleton (2002), A comparison of observed upwelling mechanisms off the east coast of Australia, *Cont. Shelf Res.*, *22*, 2551–2572.

Roughan, M., and J. H. Middleton (2004), On the East Australian Current: Variability, encroachment, and upwelling, *J. Geophys. Res.*, *109*, C07003, doi:10.1029/2003JC001833.

Roughan, M., B. D. Morris, and I. M. Suthers (2010), NSW-IMOS: An Integrated Marine Observing System for southeastern Australia. *IOP Conf. Ser.: Earth Environ. Sci.*, *11*, 012030.

Roughan, M., H. S. Macdonald, M. E. Baird, and T. M. Glasby (2011), Modelling coastal connectivity in a Western Boundary Current: Seasonal and inter-annual variability, *Deep Sea Res., Part II*, *58*(5), 628–644, doi:10.1016/j.dsr2.2010.06.004.

Schaeffer, A., M. Roughan, and B. D. Morris (2013), Cross-shelf dynamics in a Western Boundary Current regime: Implications for upwelling, *J. Phys. Oceanogr.*, *43*, 1042–1059.

Sudre J., Maes C., and V. Garçon (2013), On the global estimates of geostrophic and Ekman surface currents, *Limnol. Oceanogr. Fluids Environ.*, *3*, 1–20.

Suthers, I. M., et al. (2011), The strengthening East Australian Current, its eddies and biological effects—An introduction and overview, *Deep Sea Res., Part II*, *58*, 538–546.

Thompson, P. A., P. B. Bonham, A. M. Waite, L. A. Clementson, N. Cherukuru, and M. A. Doblin (2011), Contrasting oceanographic conditions and phytoplankton communities on the east and west coasts of Australia, *Deep Sea Res., Part II*, *58*, 645–663.

Tranter, D. J., D. J. Carpenter, and G. S. Leech (1986), The coastal enrichment effect of the East Australian Current eddy field, *Deep Sea Res., Part I*, *33*(11–12), 1705–1728.

Wood, J., M. Roughan, and P. Tate (2012), Finding a proxy for wind stress over the coastal ocean, *Mar. Fresh. Res.*, *63*, 528–544.

Zhang, H.-M., J. J. Bates, and R. W. Reynolds (2006), Assessment of composite global sampling: Sea surface wind speed, *Geophys. Res. Lett.*, *33*, L17714, doi:10.1029/2006GL027086.